

# Nuclear magnetic resonance force microscopy with a microwire rf source

M. Poggio<sup>1,2</sup>, C. L. Degen<sup>1</sup>, C. T. Rettner<sup>1</sup>, H. J. Mamin<sup>1</sup>, and D. Rugar<sup>1</sup>

<sup>1</sup>IBM Research Division, Almaden Research Center, 650 Harry Rd., San Jose CA, 95120

<sup>2</sup>Center for Probing the Nanoscale, Stanford University, 476 Lomita Hall, Stanford CA, 94305

(Dated: November 8, 2018)

We use a 1.0- $\mu\text{m}$ -wide patterned Cu wire with an integrated nanomagnetic tip to measure the statistical nuclear polarization of  $^{19}\text{F}$  in  $\text{CaF}_2$  by magnetic resonance force microscopy (MRFM). With less than 350  $\mu\text{W}$  of dissipated power, we achieve rf magnetic fields over 4 mT at 115 MHz for a sample positioned within 100 nm of the “microwire” rf source. A 200-nm-diameter FeCo tip integrated onto the wire produces field gradients greater than  $10^5$  T/m at the same position. The large rf fields from the broadband microwire enable long rotating-frame spin lifetimes of up to 15 s at 4 K.

PACS numbers: 85.85+j, 85.35.-p, 81.16.-c, 84.40.Az

The proposal of magnetic resonance force microscopy (MRFM) [1] and its subsequent realization [2] combine the physics of magnetic resonance imaging with the techniques of scanning probe microscopy. Recently this marriage has led to the demonstration of nuclear spin imaging with a spatial resolution of 90 nm [3]. In order to eventually image on the scale of single nuclear spins, the force sensitivity of the measurement must be improved by roughly 3 orders of magnitude. Such an improvement will only be achieved if the dimensions of some key components are scaled down to more closely match the nanometer and sub-nanometer length scales of single spin physics. The most recent advances in sensitivity were the result of an increase in the magnetic field gradient provided by the scanning magnetic tip. Here, we discuss MRFM measurements done with a “microwire” rf source and an integrated nanomagnetic tip meant to further scale down the measurement apparatus. The reduced heat dissipation of the compact new geometry allows us to simultaneously access temperatures under 300 mK and rf magnetic field amplitudes above 4 mT — fields large enough to produce remarkably long rotating-frame nuclear spin lifetimes.

We measure the statistical polarization [4] of  $^{19}\text{F}$  spins in a  $\text{CaF}_2$  crystal using a technique known as adiabatic rapid passage [5]. In a fixed magnetic field  $\mathbf{B}_0$ , we sweep the frequency  $\nu_{\text{rf}}$  of a transverse rf magnetic field  $\mathbf{B}_1$  through the nuclear resonance condition,  $\nu_{\text{rf}} = \frac{\gamma}{2\pi}B_0$ , where  $\gamma$  is the gyromagnetic ratio of  $^{19}\text{F}$ . If done slowly enough, i.e. if the adiabatic condition  $\partial\nu_{\text{rf}}/\partial t \ll \frac{\gamma^2}{2\pi}B_1^2$  is met, then the sweep induces nuclear spin inversions along the  $\mathbf{B}_0$  direction. We then detect these inversions using a magnetic tip and an ultrasensitive cantilever as a force detector.

The force detection apparatus, shown in Fig. 1(b), uses a sample-on-cantilever configuration. The single crystal Si cantilever is 120- $\mu\text{m}$  long, 3- $\mu\text{m}$  wide, and 0.1- $\mu\text{m}$  thick and includes a 15- $\mu\text{m}$  long, 2- $\mu\text{m}$  thick mass on its end [6]. The cantilever’s mass-loaded geometry suppresses the motion of flexural modes above the fundamental fre-

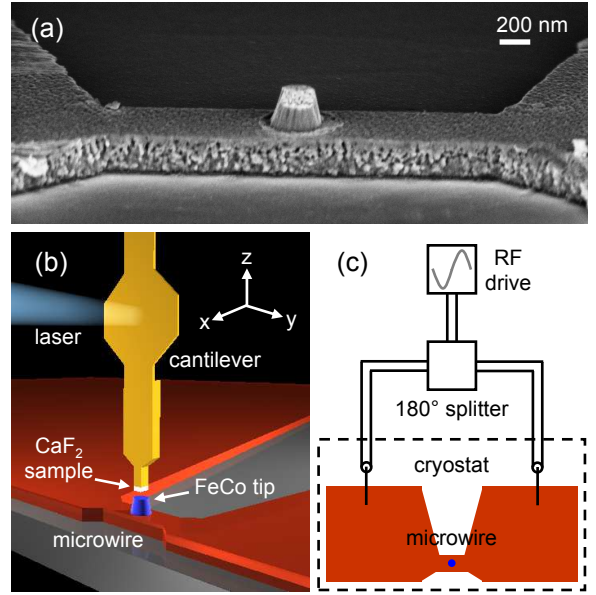


FIG. 1: (a) Scanning electron micrograph of the Cu microwire with integrated FeCo tip. (b) Representation of the experimental apparatus at the bottom of the cryostat (the relative scale of the components has been slightly altered).  $\mathbf{B}_0$ , the cantilever shaft, and the axis of the magnetic tip are aligned along  $\hat{z}$ . Current flows in the wire along  $\hat{y}$ , while at the position of the sample, the lever displacement and  $\mathbf{B}_1$  are directed along  $\hat{x}$ . (c) Schematic diagram of the electrical connections to the microwire.

quency [7, 8]. A  $\sim 50\text{-}\mu\text{m}^3$  particle of  $\text{CaF}_2$  crystal glued to the end of the lever serves as the sample. A thin layer of Si/Au (10/30 nm), with Si as an adhesion layer, is evaporated onto the end of the sample to screen electrostatic fields. At  $T = 4.2$  K the sample-loaded cantilever has a resonant frequency  $\nu_c = 2.6$  kHz and an intrinsic quality factor  $Q_0 = 44,000$ . The oscillator’s spring constant is determined to be  $k = 86$   $\mu\text{N/m}$  through measurements of its thermal noise spectrum at several different base temperatures. The cantilever is mounted in a vacuum chamber (pressure  $< 1 \times 10^{-6}$  torr) at the

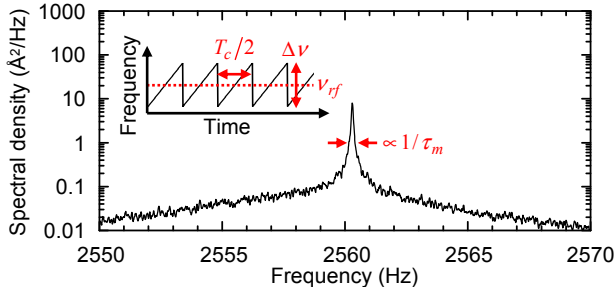


FIG. 2: The power spectral density of cantilever displacement during adiabatic rapid passage of a statistical polarization of  $^{19}\text{F}$  spins. The inset represents the frequency sweep of  $B_1$  that induces the passages.

bottom of a dilution refrigerator, which is isolated from environmental vibrations. The motion of the lever is detected using laser light focused onto a  $10\text{-}\mu\text{m}$  wide paddle near the mass-loaded end and reflected back into an optical fiber interferometer [9]. 100 nW of light are incident on the paddle from a temperature-tuned 1550-nm distributed feedback laser diode [10]. We damp the cantilever using feedback to a quality factor of  $Q = 250$  in order to increase the bandwidth of our force detection without sacrificing force sensitivity [11].

The key component of this experiment is the microwire rf source, which efficiently produces a strong rf magnetic field  $B_1$  for nuclear magnetic resonance. The Cu wire is  $2.6\text{-}\mu\text{m}$  long,  $1.0\text{-}\mu\text{m}$  wide, and  $0.2\text{-}\mu\text{m}$  thick and is patterned atop a Si substrate, as shown in Fig. 1(a). The microwire bridges the gap between two  $1\text{-mm}^2$  pads and has a resistance of  $0.35\ \Omega$  at  $T = 4.2\ \text{K}$ . In the middle of the microwire structure, deposited on its surface, is a  $250\text{-nm}$  tall,  $200\text{-nm}$  wide FeCo tip, in the shape of a truncated cone. This nanomagnetic tip provides the spatial magnetic field gradient required by the MRFM measurement.

We fabricate the microwire using lift-off, then we place the magnetic tip on the wire through a novel stencil-based process. First, a  $450\text{-nm}$  layer of IBM KRS photoresist is patterned using electron-beam lithography on a pre-scribed wafer to define the copper wire. A Cr/Cu/Au ( $5/200/5\ \text{nm}$ ) film is then deposited via thermal evaporation and lifted off in hot solvent with ultrasonic agitation. To form the magnetic tip, a  $500\text{-nm}$  thick film of polyimide is then spun onto the wafer and coated with a thin layer of evaporated Ti. A single hole is written above the wire, again with electron beam lithography, in a resist covering the Ti. The Ti is then etched with a  $\text{CF}_4$  plasma. Next we etch the polyimide with an  $\text{O}_2$  reactive ion etch through this hole to form a cavity. The resulting undercut Ti/polyimide bilayer structure forms a stencil mask over the wire onto which the magnetic film can be evaporated. This film consists of Ti/ $\text{Co}_{30}\text{Fe}_{70}$ /Au ( $15/200/15\ \text{nm}$ ) deposited by e-beam

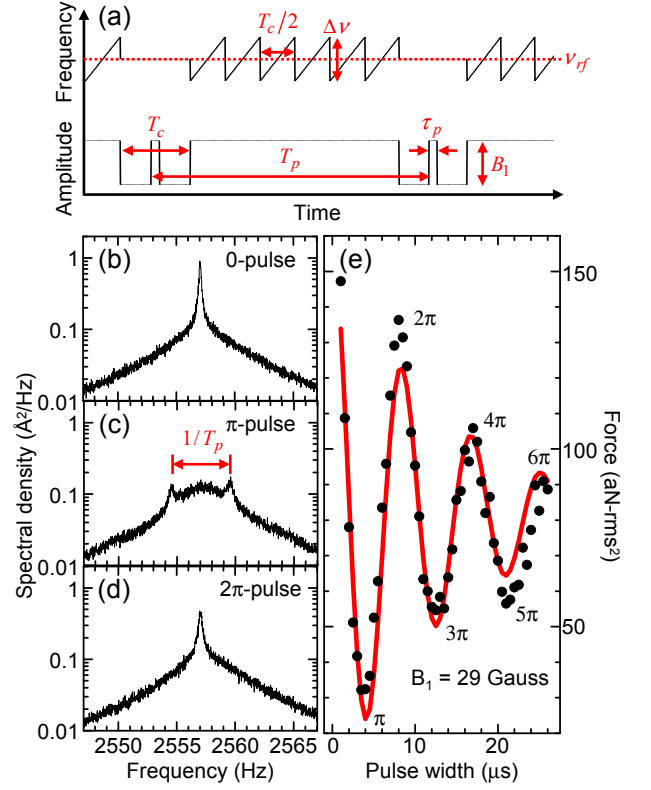


FIG. 3: (a) The rf pulse protocol for the spin nutation experiment. The resulting power spectral density of cantilever displacement with pulse widths  $\tau_p$  equivalent to (b) 0, (c)  $\pi$ , and (d)  $2\pi$  radians of nutation. (e) The corresponding force signal is measured through a narrow band lock-in amplifier and plotted in points as a function of pulse width  $\tau_p$ . A  $B_1$  amplitude can be extracted from a decaying cosinusoidal fit of the Rabi oscillations shown in red.

evaporation. All the Au capping layers are meant to provide protection against oxidation. After final lift-off, the wafer is cleaved along the pre-existing scribe in order to place the wire less than  $50\ \mu\text{m}$  from the edge of the chip. The structure's proximity to the edge ensures a clear optical path from the fiber interferometer to the cantilever paddle.

The overall geometry of the MRFM apparatus is shown in Fig. 1(b). During measurement, the sample at the end of the cantilever is situated less than  $100\ \text{nm}$  directly above the nanomagnetic tip. At such a small spacing, the magnetic tip provides fixed spatial field gradients in excess of  $10^5\ \text{T/m}$ . Less than  $20\ \text{mA}$  passing through the microwire (current density  $\sim 10^7\ \text{A/cm}^2$ ) produce rf  $B_1$  fields larger than  $4\ \text{mT}$  (rotating field) at the position of the sample. Under these conditions, the heat dissipated by the wire is under  $350\ \mu\text{W}$  allowing the dilution refrigerator to reach temperatures below  $300\ \text{mK}$ . The rf current required to produce  $B_1$  flows through the microwire from the pads on either side of it. These pads are each connected through short Cu leads to the center conduc-

tors of semi-rigid coaxial lines leading to the top of the cryostat. The two lines are differentially driven by a  $180^\circ$  splitter, which is in turn connected to the rf drive signal as shown in Fig. 1(c). By matching the attenuation and delay caused by each coaxial line, this differential driving scheme results in a voltage node and a current anti-node at the microwire. In this way, we maximize the rf magnetic field produced around the microwire while minimizing unwanted electric fields, which could cause spurious excitation of our cantilever. Note that since the wire is not frequency-specific it has the flexibility of being a broadband source of rf magnetic field. In the present experiment, the upper frequency limit is about 200 MHz due to the inductance of the wire leads.

In typical MRFM measurements of the  $^{19}\text{F}$  spin polarization by adiabatic rapid passage, we drive the microwire with the frequency-sweep waveform represented in the inset to Fig. 2. In these experiments we use a center frequency  $\nu_{\text{rf}} = 114.7$  MHz and a peak-to-peak frequency deviation  $\Delta\nu = 1.4$  MHz. A superconducting magnet provides the resonant field for  $^{19}\text{F}$  of  $B_0 \simeq 2.9$  T. By generating an rf magnetic field whose frequency is swept through the  $^{19}\text{F}$  resonance twice every cantilever period  $T_c$ , we drive longitudinal nuclear spin flips in the sample at the lever's resonance frequency. Since the sample is mounted on the end of the cantilever, in the presence of a large enough magnetic field gradient, the spin flips produce a force that drives the lever. By measuring the amplitude of the cantilever's oscillation on resonance we determine the longitudinal component of net spin polarization. In our case, this polarization is due to the naturally occurring  $\sqrt{N}$  statistical component. The cantilever displacement induced by adiabatic passages is shown in the vibrational spectrum plotted in Fig. 2. The narrow band spin signal, whose spectral width is inversely proportional to the rotating-frame spin lifetime  $\tau_m$ , sits atop a much broader peak generated by the lever's natural thermal vibrations.

To measure the magnitude of  $B_1$ , which the microwire produces in the sample, a different rf protocol, shown schematically in Fig. 3(a), is used. We sweep the frequency  $\nu_{\text{rf}}$  of  $B_1$  through resonance twice per cantilever period, as discussed previously, and intersperse the frequency sweeps with occasional resonant pulses of variable width  $\tau_p$ , spaced by  $T_p$ . Here we use  $T_p = 196$  ms or  $502 \times T_c$ . Given a fixed amplitude  $B_1$ , as we increase  $\tau_p$ , the resonant pulses induce spins to nutate with an increasing angle. If the pulse spacing is much less than the rotating-frame spin lifetime,  $T_p \ll \tau_m$ , nutations produced by the pulses modulate the force signal generated by the adiabatic passages. When  $\tau_p = \pi/(\gamma B_1)$ , i.e. the pulse width and amplitude is equivalent to  $\pi$  radians of nutation, each pulse reverses the sign of the force signal. This modulation results in sidebands appearing in the frequency spectrum of the cantilever displacement signal spaced by  $1/(2T_p)$  from the lever resonance at  $\nu_c$ .

The signal power formerly in the central peak shifts to the sidebands and back again depending on the rf pulse width  $\tau_p$ , as shown in Fig. 3(b)-(d). By feeding the displacement signal into a narrow band lock-in amplifier referenced to  $\nu_c$ , we measure the power at  $\nu_c$  as a function of  $\tau_p$  and observe the Rabi oscillations plotted in Fig. 3(e). From the period of these oscillations we extract the pulse width required for  $2\pi$  radians of nutation,  $\tau_{2\pi}$ . Using the relation  $B_1 = 2\pi/(\gamma\tau_{2\pi})$ , we determine the magnitude of  $B_1$  produced by the microwire at the sample position. Acquiring data similar to those shown in Fig. 3(e) taken at different rf drive amplitudes, we calibrate the magnitude of  $B_1$  at the sample position corresponding to a given rf drive.

In order to investigate the dependence of  $\tau_m$  for  $^{19}\text{F}$  nuclei in  $\text{CaF}_2$  as a function of increasing rf magnetic field  $B_1$ , we employ the adiabatic sweep waveform without the interspersed pulses, shown in the inset to Fig. 2. As plotted in Fig. 4,  $\tau_m$  strongly increases with increasing  $B_1$  amplitude up to a saturation around  $\tau_m = 15$  s at  $B_1 = 3$  mT. Previous low-temperature nuclear MRFM experiments were done with  $B_1 < 2$  mT due to the large heat dissipation caused by the larger than  $100\text{-}\mu\text{m}$ -diameter coils used as rf sources [3]. These conditions resulted in  $\tau_m < 500$  ms. In this low  $B_1$  regime, rotating-frame lifetimes are often very short due to either violation of the adiabatic condition [12], spin-spin interactions, or spin relaxation caused by the thermal vibration of higher order cantilever modes in the strong field gradients provided by the nanomagnetic tip [7, 8].

In addition to the newly accessible regime of long  $\tau_m$ , the small amount of heat dissipated by the microwire — even for large  $B_1$  amplitudes — is the fundamental advance presented here. Previous nuclear MRFM experiments were done with a hand-wound coil larger than  $200\text{ }\mu\text{m}$  in diameter as an rf source; the coil produced less than 2 mT at the sample with more than 200 mW of dissipated heat. In contrast, since our microwire can be less than 100 nm from the sample, it produces more than

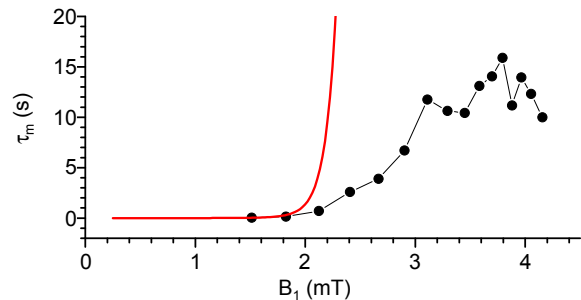


FIG. 4: Plot of the  $\tau_m$  as a function of  $B_1$  in the sample at  $T = 4.2$  K. Red line corresponds to the limit set on  $\tau_m$  by the adiabatic condition and is calculated using numerical integration of the Bloch equations for repetitive linear frequency sweeps of  $\nu_{\text{rf}}$  through resonance [13].

4 mT with less than 350  $\mu$ W of dissipated heat.

We thank M. Hart and M. Farinelli for assistance with magnetic tip fabrication. We acknowledge support from the DARPA QuIST program administered through the Army Research Office, the NSF-funded Center for Probing the Nanoscale (CPN) at Stanford University, and the Swiss National Science Foundation.

- 
- [1] J. A. Sidles, *Phys. Rev. Lett.* **68**, 1124 (1992).
  - [2] D. Rugar, C. S. Yannoni, and J. A. Sidles, *Nature* **360**, 563 (1992).
  - [3] H. J. Mamin, M. Poggio, C. L. Degen, and D. Rugar, *Nature Nanotechnology* **2**, 301 (2007); [cond-mat/0702664](#).
  - [4] H. J. Mamin, R. Budakian, B. W. Chui, and D. Rugar, *Phys. Rev. Lett.* **91**, 207604 (2003).
  - [5] C. P. Slichter, *Principles of Magnetic Resonance* (Springer-Verlag, New York, 1990), 3rd ed., Chaps. 2 and 6.
  - [6] B. W. Chui *et al.*, *Technical Digest of the 12th International Conference on Solid-State Sensors and Actuators (Transducers '03)*, (IEEE Boston, MA, 2003), p. 1120.
  - [7] D. Mozyrsky, I. Martin, D. Pelekhov, and P. C. Hammel, *Appl. Phys. Lett.* **82**, 1278 (2002).
  - [8] G. P. Berman, V. N. Gorshkov, D. Rugar, and V. I. Tsifrinovich, *Phys. Rev. B* **68**, 094402 (2003).
  - [9] D. Rugar, H. J. Mamin, and P. Guethner, *Appl. Phys. Lett.* **55**, 2588 (1989).
  - [10] K. J. Bruland *et al.*, *Rev. Sci. Instr.* **70**, 3542 (1999).
  - [11] J. L. Garbini, K. J. Bruland, W. M. Dougherty, and J. A. Sidles, *J. Appl. Phys.* **80**, 1951 (1996); K. J. Bruland, J. L. Garbini, W. M. Dougherty, and J. A. Sidles, *J. Appl. Phys.* **80**, 1959 (1996).
  - [12] C. W. Miller and J. T. Markert, *Phys. Rev. B* **72**, 224402 (2005).
  - [13] J. Baum, R. Tycko, and A. Pines, *Phys. Rev. A* **32**, 3435 (1985).